Processing and characterization of alumina thin films on chemically vapor deposited diamond substrates for producing adherent metallizations

E. S. K. Menon and I. Dutta
Department of Mechanical Engineering, Center for Materials Science and Engineering, Naval Postgraduate School, Monterey, California 93943

(Received 11 August 1997; accepted 27 April 1998)

In order to make the surface of chemically vapor deposited diamond (CVDD) substrates amenable to metallization by both thin and thick film approaches currently utilized in electronic packaging, a thin, adherent, insulating aluminum oxide film was grown on diamond at low temperatures (<675 K). The film was produced by reactive thermal evaporation of Al and O in an oxygen atmosphere, followed by low-temperature annealing in oxygen. A Cr intermediate layer was deposited on diamond prior to the deposition of aluminum oxide in order to enhance adhesion between the oxide and diamond. The chemistry, crystal structure, and microstructure of the film were characterized in detail via scanning and transmission electron microscopy, as well as Auger electron spectroscopy. Particular attention was given to the mechanisms of bonding across the CVDD-Cr and Cr-alumina interfaces, as well as the stability of the surface treatment following metallization by fritted pastes requiring firing at elevated temperatures. The Cr was found to be bonded with CVDD by $Cr_{23}C_6$ formation, while the bonding between the Cr and alumina layers was provided by the formation of a compositionally modulated solid solution with Al_2O_3-rich and Cr_2O_3-rich regions.

I. INTRODUCTION

Chemically vapor deposited (CVD) diamond is very attractive as a substrate material for electronic packaging[1] because of its excellent thermal conductivity (1500–2000 W/m-K), high electrical resistivity (10^{13}–10^{14} Ω-cm), low dielectric constant (5.6), and low loss tangent (0.0005). However, typical conductive metallizations, such as gold (Au), copper (Cu), and aluminum (Al), display very poor adhesion to diamond, thereby causing problems associated with the reliability and stability of metallized diamond packages. Additionally, the large difference between the thermal expansion coefficient of diamond ($\sim 1-2 \times 10^{-6}$/K) and most metals ($15-20 \times 10^{-6}$/K) results in the generation of large residual stresses in most metallizations, leading to problems associated with peeling and/or cracking of the metallization. As a result, standard thin or thick film techniques utilized in metallizing ceramic substrates are not suitable for use on diamond.

Several processes for metallizing diamond have been proposed recently.[2–7] All these processes involve the application of a transition metal, either as the final metallization or as an intermediate layer between CVD diamond and the conductive metallization. Typical metals used for this purpose include Ti, W, Cr, Nb, Ta, or an alloy (e.g., W-Ti). In each case, the selected metal is a strong carbide former, and is believed to bond with diamond via metal-carbide formation at the interface. A separate final conductive metallization (e.g., Au), where necessary, is subsequently applied on the interlayer to form the interconnection circuitry via a thin or thick film process, and adheres to the interlayer via metallic bonding.

The above approach either produces a metallization with less than ideal electrical properties (since the transition metals have considerably lower electrical conductivity than metallizations such as Au, Cu, or Al), or requires that the interlayer be patterned identically to the overlying interconnection circuitry. This requirement for patterning the interlayer complicates the metallization process substantially, and in practice, restricts the use of such approaches to thin film/lithographic techniques, making it unsuitable for conventional thick film processes based on screen printing of fritted pastes. Since both thin and thick film metallization approaches are currently in wide use in the electronic packaging industry, there is a need to develop alternate approaches to metallize diamond.

A new surface modification approach for CVD diamond in order to make it suitable for both thin and thick film metallization was recently proposed.[8,9] In this approach, a thin (10–50 nm) film of Cr was thermally evaporated onto a heated diamond substrate, followed by deposition of a 50–150 nm thick Al_2O_3 layer on top of it by reactive thermal evaporation. Following an appropriate annealing treatment in an oxygen-rich environment, the surface of the coated diamond substrate was found to consist almost entirely of nanocrystalline γ–Al_2O_3.

Alumina was chosen as the final surface layer because of its current popularity as a substrate material for electronic packaging, and the consequently wide availability of metallization approaches for it. Additionally, it has a coefficient of thermal expansion intermediate between those of diamond and the final metallization, and should therefore reduce interfacial residual stresses and thereby enhance package reliability. Although Al_2O_3 has a much lower thermal conductivity (~25 W/m-K) than diamond, the reduction in thermal conductivity due to the alumina layer may be minimized by keeping the layer thin. For instance, a simple one-dimensional heat transfer calculation reveals that the through-thickness thermal conductivity of a 200 micrometers (μm) thick diamond of K = 1500 W/m-K drops by less than 3% upon being coated with a 100 nm thick layer of alumina.[9]

Qualitative adhesion tests demonstrated good adhesion between the alumina and the diamond layer through the Cr interlayer,[8,9] and it was surmised that the Cr bonds with diamond through interfacial carbide formation, whereas the alumina and the Cr bond via solid-solution formation. However, the exact nature of the two interfaces was not clear from previous work. Further, it was observed that both the post-deposition annealing treatment and the presence of the Cr interlayer were critical components of an adherent, electrically insulating surface modification for diamond. Therefore, it is crucial to develop a mechanistic understanding of the role of each in order to optimize the processing conditions for the proposed surface treatment.

Adherent oxide films have been deposited on a variety of organic and inorganic substrates by a number of deposition techniques.[10–20] The general approach comprises physical or chemical vapor deposition of the appropriate species, followed by a heat treatment in the presence of either oxygen or water vapor, during which the microstructure and properties of the film evolve. In most cases, the as-deposited film is amorphous, but can be made to crystallize partially following a suitable treatment.[10,11] Reactive evaporation has been successfully utilized to deposit Al_2O_3 films,[12,16,17] although the oxidation of Al to Al_2O_3 is usually not complete in the as-deposited condition,[12,16] making the film properties change during subsequent environmental exposure. Both temperature and rate of deposition play important roles in determining the final composition and structure of the deposited film, with the structure changing from amorphous Al_2O_3 to cubic $\gamma-Al_2O_3$ to hexagonal $\alpha-Al_2O_3$ with the temperature increasing from 973 K to 1473 K, and the stoichiometry changing from Al–O with excess Al to Al_2O_3 with a reduction in deposition rate.[12] Although amorphous Al_2O_3 films may have acceptable electrical resistivity and breakdown characteristics for certain niche applications, their capacitance-voltage characteristics are generally inadequate for use as dielectrics.[11] Therefore, for the present application (surface treatment on diamond), it is important to have a reliable method of producing crystalline Al_2O_3. To date, no study (except Refs. 8 and 9 by the present authors) has reported on the deposition of Al_2O_3 on diamond. In particular, no work on alumina deposition on diamond by reactive evaporation of Al in the presence of oxygen has been reported, since the production of crystalline alumina by evaporation has so far not been possible at temperatures below 973 K, and diamond oxidizes rapidly at temperatures above 873 K.

Although Cr has been previously utilized as an adhesion-enhancing intermediate layer between an oxide film (SiO_2) and a polymeric substrate (diethyl glycol bis allyl carbonate),[10] the precise role of Cr in adhesion-enhancement and/or nucleation-and-growth of an overlying oxide film has not been studied. A recent AES study of the interface between Cr film thermally evaporated at very slow rate (~0.4 nm/min) onto an Al_2O_3 substrate in ultrahigh vacuum has shown that during deposition, Cr atoms get oxidized upon contacting the surface of Al_2O_3, thereby producing metallic Al on the substrate surface by the reduction of Al^{+3}.[21] The interfacial reaction, which was thought to occur[21] by charge transfer from the Cr-3*d* to the O-2*p* orbitals, thereby forming chromium oxide at the interface, is responsible for the strong adhesion between Cr and Al_2O_3. Thus, it was concluded that the interface between Cr and Al_2O_3 consists of either a double oxide or two separated oxides of Cr and Al, as well as some metallic Al.[21] However, it is not clear whether the mechanism of bonding remains the same when Al and O are reactively deposited on metallic chromium, as in the present study.

Several studies have reported on the bonding of diamond with various transition elements.[22–27] Investigations of the interface between diamond deposits and Ti, Ni, and Si substrates have revealed the presence of several metal-C and Si-C phases, which often contain oxygen and may be amorphous or crystalline.[22–25] Detailed x-ray photoelectron spectroscopy (XPS) and Auger electron spectroscopy (AES) studies[26] of the interface between a Ti film and a diamond substrate have shown that the as-deposited Ti film has minimal chemical interaction with diamond and produces a rectifying electrical contact, whereas after annealing, an ohmic contact is produced due to the formation of interfacial carbides. Bonding of intermediate layers of a transition and/or refractory metal (between a final metallization and diamond) by carbide formation with the diamond substrate has been noted in several studies.[2,27–30] Recent work on metallization of diamond with various transition-metal intermediate layers[27] has shown that the interlayer-diamond interface is quite stable at low temperatures, but degrade rapidly by extensive carbide formation and oxidation of the interlayer. To date, only one study

has reported on the use of a Cr interlayer between diamond and the final Au metallization.[30] However, the precise stoichiometry of the Cr-diamond interface was not investigated in detail in this study,[30] although it was noted that annealing at higher temperatures (723 K vs 573 K) results in greater interdiffusion across the interface. It was further noted that during the evaporative deposition of Cr at rates as rapid as 60 nm/min at a base pressure of 10^{-6} Torr, the Cr droplets undergo partial oxidation prior to incidence on the substrate surface, thereby stabilizing the Cr layer and inhibiting its diffusion into the overlying Au layer.[30]

The purpose of this paper is to report on the processing and characterization of polycrystalline alumina films grown on a Cr-coated CVD diamond substrate by low-temperature reactive evaporation. Of particular interest are the structure of the alumina film, the mechanism of bonding of the film with the underlying Cr layer, the mechanism of bonding across the Cr-diamond interface, and the chemistry of the layered system. Special emphasis has been placed on delineating the roles of the Cr interlayer and the annealing process in the evolution of the structure and properties of the alumina film. It is believed that a detailed understanding of the present system will not only allow the production of reliable surface metallizations on diamond by all existing thin- and thick-film techniques, but also enable the design and processing of alternating metal-dielectric multilayered schemes for diamond-based electronic packages.

II. EXPERIMENTAL

The diamond substrates used for the experiments were processed by microwave plasma-assisted chemical vapor deposition at the Naval Air Warface Center, Indianapolis, IN. The diamond films, which possessed a strong ⟨100⟩ texture, were 70–100 μm thick, and were deposited on either Si or AlN substrates. The as-received diamond surface was cleaned with tri-chloro-ethylene, acetone, and ethanol, and dried. The cleaned diamond substrate was then baked at 623–673 K for 5 h in vacuum (base pressure, P_b, of 2×10^{-7} Torr) prior to deposition. Subsequently, a 20–50 nm thick layer of Cr (Cr chips, 99.9% pure) was thermally evaporated onto the diamond at a deposition rate of 10 nm/min. This was followed by the deposition of a 100–200 nm thick alumina layer by reactive evaporation of Al (Al wire, 99.99% pure) and 99.99% pure oxygen at an oxygen partial pressure (P_{O_2}) of $\sim 10^{-4}$ Torr. Following backfilling with oxygen, the total chamber pressure $P_{\text{total}} \approx P_{O_2}$ since $P_b \ll P_{O_2}$. The deposition rate was 4 nm/min. During all stages of deposition, the temperature of the diamond substrate surface was maintained at 573–673 K. Following deposition, an annealing treatment (400 °C for 24 h) was carried out in oxygen atmosphere after backfilling the deposition chamber with oxygen to a pressure of ~500 Torr. This procedure was found to provide well-adherent alumina films on CVDD, as verified by qualitative adhesion tests using replicating acetate tape as well as Scotch™ packaging tape.[8,9] Because of the good adhesion between the alumina film and CVDD, it is expected that any thin or thick film metallization approach suitable for alumina substrates will produce well-bonded metallizations on the surface modified CVDD.

A few control films were also deposited on borosilicate glass slides, as well as on freshly cleaved {100} surfaces of single crystal NaCl substrates following exactly the same procedure as above. The films on borosilicate glass were utilized for the measurement of electrical resistivity. Resistance measurements were conducted using the four-point method in order to eliminate contact resistances, using a constant current source and high-resolution voltmeter. The films deposited on NaCl were subsequently separated from the substrate by dissolving the NaCl in water, and were examined in a TOPCON 002B transmission electron microscope (TEM) equipped with an energy dispersive x-ray spectroscope (EDS) and an electron energy loss spectroscope (EELS). Some of the control films were deposited either (i) without a Cr interlayer or (ii) without the post-deposition annealing treatment, with the aim of understanding the roles of these two parameters on the structure and properties of the surface film.

In order to study in detail the Cr-diamond interface, separate samples were produced wherein 20–40 nm thick Cr films were deposited on clean diamond substrates following the procedure outlined above. Following deposition, the sample was annealed at 673 K in vacuum for 24 h. The Cr-diamond interface was then characterized in detail by Auger electron spectroscopy by depth profiling and collecting complete Auger electron spectra following sputtering to various depths. AES was also utilized in order to conduct detailed chemical characterization of the entire Al_2O_3–Cr-diamond system. In order to investigate the stability of the surface modification during metallization firing, cross-sectional samples for scanning electron microscopy (SEM) were prepared following metallization of the alumina-coated diamond using a commercial fritted silver paste (FERRO 3350™) fired in argon at 725 K for 10 min. Fritted pastes for metallization typically contain several ceramic constituents which together form a low-melting eutectic at the firing temperature, thereby forming a liquid phase that penetrates the substrate surface by some distance and provides adhesion.

A separate cross-sectional TEM specimen was prepared and inspected following metallization of the alumina coated diamond substrate using a commercial fritted gold paste (DuPont DC101™), which was fired in an argon environment for 15 min at 1075 K. The

purpose of the thick film metallization studies using Ag and Au pastes was primarily to demonstrate the stability of the proposed surface modification under particularly aggressive environmental conditions (i.e., the presence of molten frits and high temperatures during the curing process).

III. RESULTS AND DISCUSSION

A. Electrical resistivity

The electrical resistivity of the thin films were determined in order to assess the quality of the films, and only the processing parameters leading to electrically insulating thin films were employed in subsequent studies. Table I summarizes the electrical resistivities determined for several alumina films deposited on borosilicate glass substrates. The data represent an average of five measurements from at least two separate films, and had a standard deviation of less than 15% in each case. For comparison, resistivity of a sample with a 60 nm thick Cr film only is reported in the table. For reference, the resistivities of bulk Cr and alumina are 1.55×10^{-6} Ω-cm and $\sim 10^{6}$ Ω-cm, respectively.

From this table we can make several interesting observations. First, the relatively high electrical resistivity of the as-deposited sample B (as compared with that of A, which has only metallic Cr) suggests that reactive deposition of Al at low substrate temperatures leads to the formation of a significant amount of alumina. Post-deposition annealing (sample C) leads to a fourfold increase in resistivity, and the introduction of a thin layer of metallic Cr prior to the reactive evaporation of Al, as in sample D, results in an even larger (in this case, fivefold) increase in electrical resistivity. A combination of the Cr intermediate layer and a post-deposition annealing heat treatment consistently produces thin films that are always insulating, as can be seen from samples E to G. Thus it is clear that the deposition of a thin layer of Cr, along with a post-deposition annealing heat treatment, offers the means to produce electrically insulating alumina films by reactive thermal evaporation even at low substrate temperatures (<675 K). Similar results were also obtained on {100} Si substrate surfaces. Hence, this procedure was adapted for further studies on surface modification of CVDD substrates. Electrical resistivity measurements were not conducted on the alumina films deposited on diamond because of the surface roughness (~5–10 μm Ra) of CVD diamond films. The results obtained here indicate that both the Cr-interlayer and the post-deposition annealing treatment play a significant role in the stability of the insulating oxide film produced. This aspect will be examined in more detail later.

B. Microstructure

Here, some qualitative observations on the microstructural characteristics of the alumina thin films are reported. Secondary electron images revealed that the annealed thin films on all substrates were characterized by rather rough surfaces with large aggregates of alumina decorating them as illustrated by an example in Fig. 1(a) that illustrates the alumina film surface formed on a freshly cleaved {100} NaCl substrate. These aggregates presumably formed during the annealing treatment due to grain coalescence enhanced by surface diffusion. Figure 1(b) shows the appearance of an alumina film produced on {100} diamond film deposited on polycrystalline AlN. As noticeable in the figure, because of the high surface roughness (~5 μm Ra) of the diamond substrate, the alumina film is uneven, although the film is continuous on each of the flat {100} faces of the diamond crystallites. Figure 1(c) shows the appearance of the alumina film produced on {100} diamond on {100} Si. Here, because of the relative smoothness of the diamond surface (<1 μm Ra), a continuous alumina film is formed on the diamond surface. In both cases [Figs. 1(b) and 1(c)], aggregates of alumina, similar to those observed on NaCl, were also present. However, the average size of the aggregates on the {100} diamond faces was noticed to be much finer than those on NaCl. TEM examinations of the alumina films (deposited on NaCl substrate) showed them to be microstructurally homogeneous and mostly comprised of nanocrystalline (3 to 10 nm) grains though occasionally larger (~25 nm) grains were also present, as illustrated in Fig. 2(a). Selected area diffraction (SAD) patterns obtained from

TABLE I. Electrical resistivities of various films deposited on borosilicate glass.

Sample	Thickness of Cr film (nm)	Thickness of Al_2O_3 film (nm)	Heat treatment	Resistivity (Ω-cm)
A	60	...	...	1.55×10^{-4}
B	...	168	...	1.3
C	...	180	24 h at 595 K	5.4
D	25	100	...	6.3
E	25	100	24 h at 625 K	Beyond instrument level (BIL)[a]
F	50	50	24 h at 595 K	BIL[a]
G	75	125	24 h at 625 K	BIL[a]

[a]Instrumental detection limit of resistance = 30 MΩ.

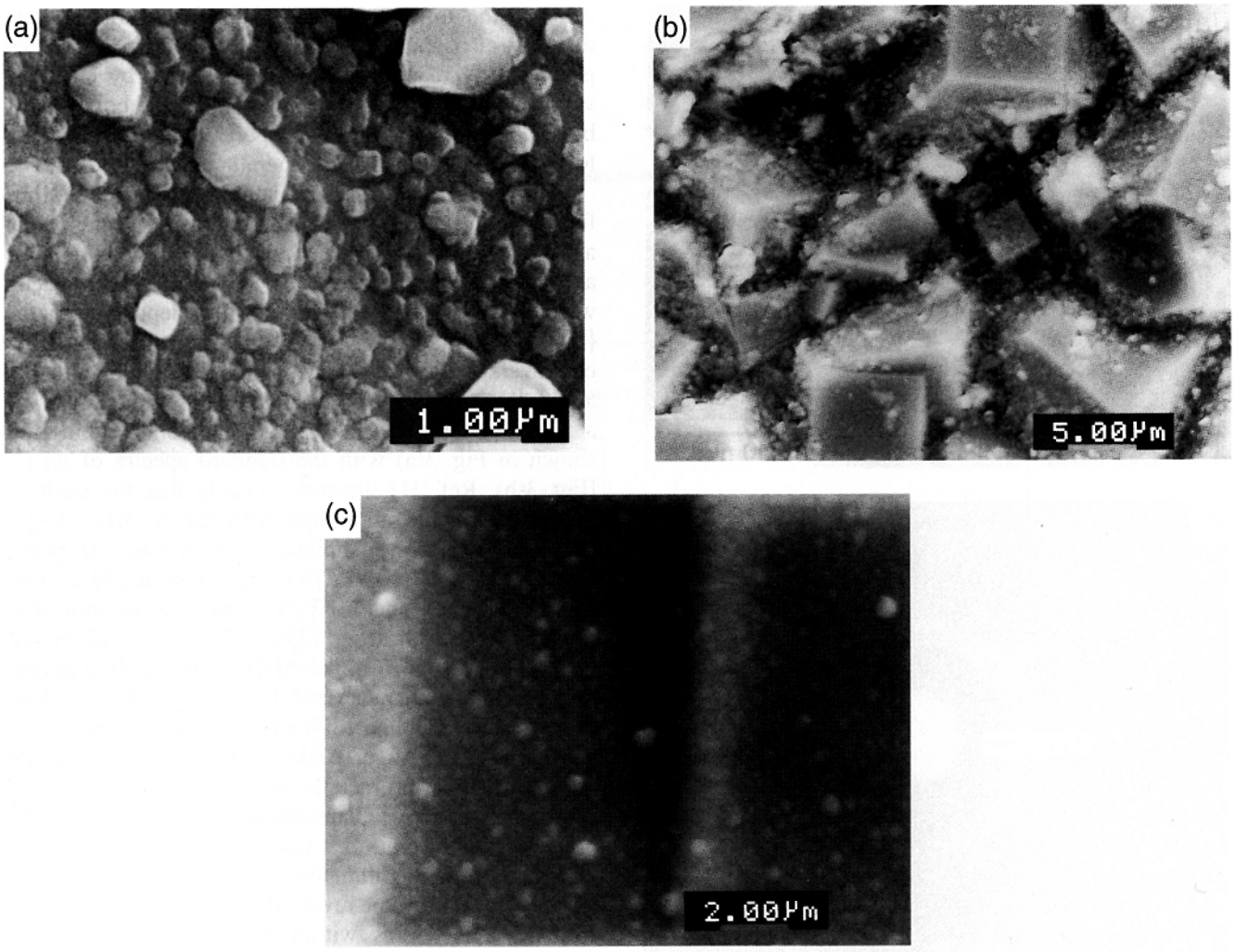

FIG. 1. (a) Secondary electron image showing the surface of the alumina film. The sample comprises of 25 nm Cr/75 nm alumina deposited on freshly cleaved {100} surface of a NaCl crystal held at 673 K during deposition and annealed at 673 K for 24 h under an oxygen pressure of 500 Torr. Notice the large agglomerates of alumina formed on the surface of the alumina thin film. (b) A low magnification secondary electron image illustrating the appearance of the alumina film on CVDD substrate. 75 nm Cr/125 nm alumina thin film deposited on CVDD was deposited at 573 K on an AlN substrate and annealed at 573 K for 24 h. {100} faces of the diamond crystals can be clearly seen here. Notice that the alumina film covers the entire rough surface of the CVDD sample. Large agglomerates of alumina can also be seen here. (c) A higher magnification secondary electron image taken from the {100} surface of a diamond crystal showing a continuous layer of alumina thin film on this surface. Much finer aggregates of alumina are seen here as compared to (a).

the as-prepared thin films were characterized by a series of continuous rings corresponding to the spacing of reflections from polycrystalline cubic $\gamma-Al_2O_3$. Following annealing, the rings corresponded to the same interplanar spacings, but were sharper and spottier [Fig. 2(b)]. The observation of spotty rings in the annealed samples is indicative of grain growth of the alumina crystals during the post-deposition heat treatment. The above suggests that crystalline $\gamma-Al_2O_3$ substantially forms during the deposition process, while the annealing treatment primarily equilibrates and coarsens the microstructure. Since the electrical resistivity (Table I) is seen to rise considerably following annealing, it is reasonable to infer that in the as-deposited form, not all locations of the film have stoichiometric crystalline alumina. The annealing process is therefore crucial in the equilibration of the film chemistry, and the optimization of its electrical properties.

C. Crystal structure

Selected area electron diffraction patterns [e.g., Fig. 2(b)] obtained from various samples established that all the observed reflections could be satisfactorily indexed as those of cubic $\gamma-Al_2O_3$ while intensities from the trigonal $\alpha-Al_2O_3$ phase were not present. The first seven observed rings are indexed in this pattern while the intensities of the rest of the rings were too low

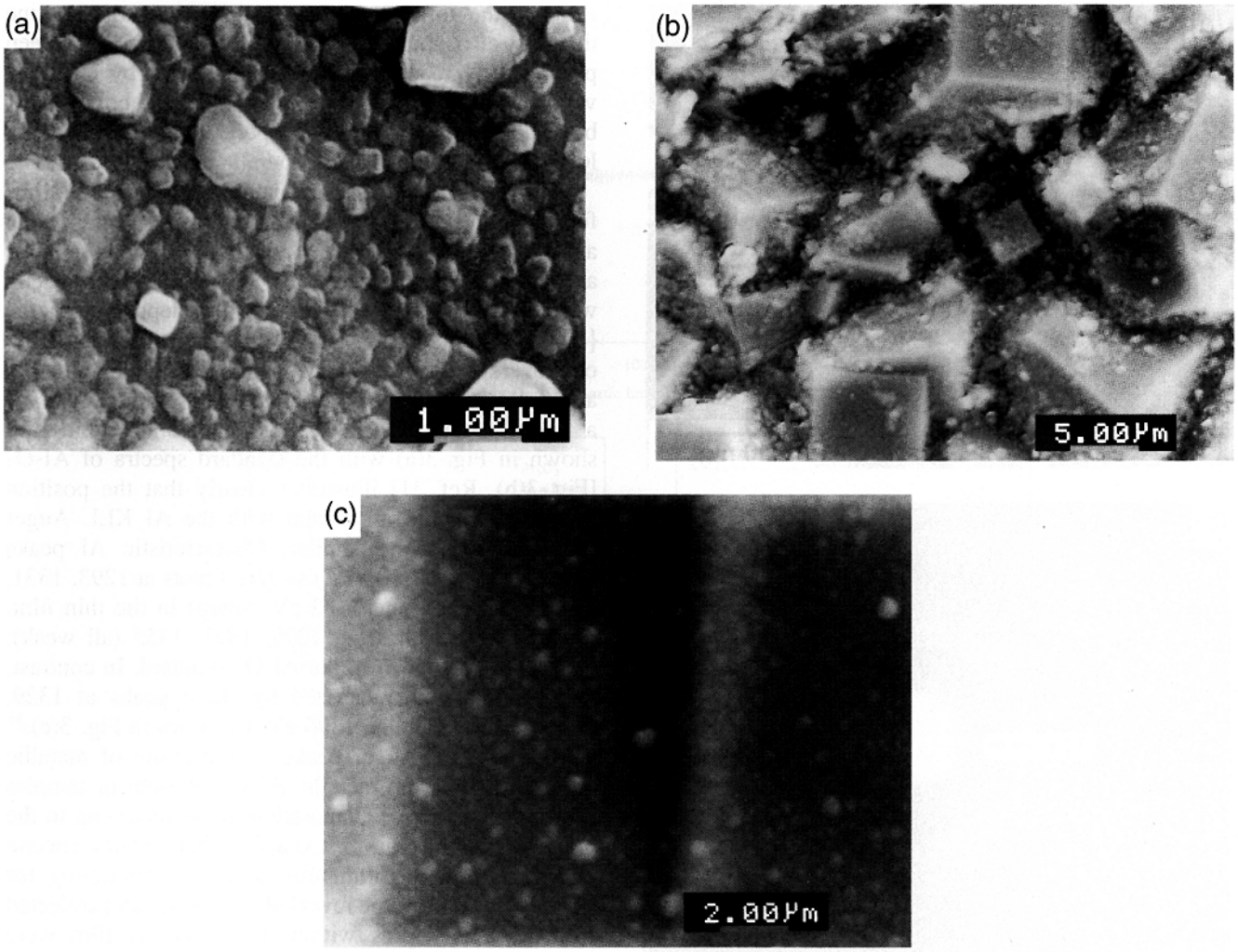

FIG. 1. (a) Secondary electron image showing the surface of the alumina film. The sample comprises of 25 nm Cr/75 nm alumina deposited on freshly cleaved {100} surface of a NaCl crystal held at 673 K during deposition and annealed at 673 K for 24 h under an oxygen pressure of 500 Torr. Notice the large agglomerates of alumina formed on the surface of the alumina thin film. (b) A low magnification secondary electron image illustrating the appearance of the alumina film on CVDD substrate. 75 nm Cr/125 nm alumina thin film deposited on CVDD was deposited at 573 K on an AlN substrate and annealed at 573 K for 24 h. {100} faces of the diamond crystals can be clearly seen here. Notice that the alumina film covers the entire rough surface of the CVDD sample. Large agglomerates of alumina can also be seen here. (c) A higher magnification secondary electron image taken from the {100} surface of a diamond crystal showing a continuous layer of alumina thin film on this surface. Much finer aggregates of alumina are seen here as compared to (a).

the as-prepared thin films were characterized by a series of continuous rings corresponding to the spacing of reflections from polycrystalline cubic $\gamma-Al_2O_3$. Following annealing, the rings corresponded to the same interplanar spacings, but were sharper and spottier [Fig. 2(b)]. The observation of spotty rings in the annealed samples is indicative of grain growth of the alumina crystals during the post-deposition heat treatment. The above suggests that crystalline $\gamma-Al_2O_3$ substantially forms during the deposition process, while the annealing treatment primarily equilibrates and coarsens the microstructure. Since the electrical resistivity (Table I) is seen to rise considerably following annealing, it is reasonable to infer that in the as-deposited form, not all locations of the film have stoichiometric crystalline alumina. The annealing process is therefore crucial in the equilibration of the film chemistry, and the optimization of its electrical properties.

C. Crystal structure

Selected area electron diffraction patterns [e.g., Fig. 2(b)] obtained from various samples established that all the observed reflections could be satisfactorily indexed as those of cubic $\gamma-Al_2O_3$ while intensities from the trigonal $\alpha-Al_2O_3$ phase were not present. The first seven observed rings are indexed in this pattern while the intensities of the rest of the rings were too low

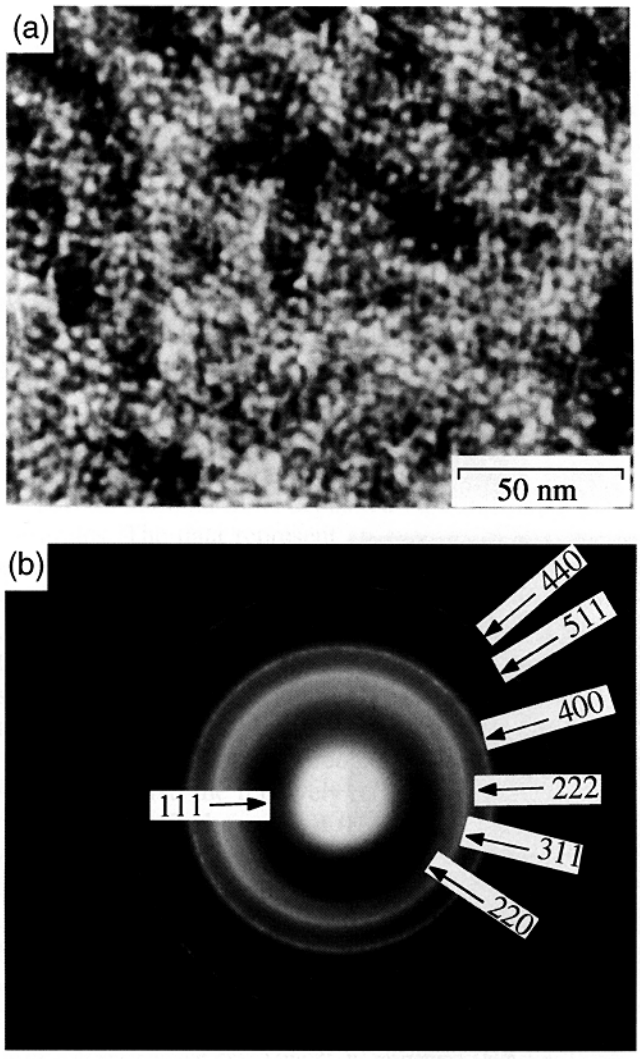

FIG. 2. Microstructure of the alumina film deposited on a 20 nm Cr interlayer. This film was deposited on a freshly cleaved {100} surface of a NaCl crystal, which was subsequently dissolved in water to separate the film from the substrate. (a) Bright-field image showing fine 3–10 nm sized grains. (b) The corresponding SAD pattern reveals that the film consists of numerous ultrafine, misoriented $\gamma-Al_2O_3$ crystallites. The first seven sharp rings have been indexed according to the $\gamma-Al_2O_3$ crystal structure.

and cannot be seen in the photographic print. Although the diffraction rings appear to be continuous, a careful examination shows that the rings actually are composed of diffraction spots as indicated earlier. This is suggestive of fine-grained crystallites in the thin film, consistent with the microstructural observation mentioned earlier of nanometer-sized grains forming the thin film samples. EDS analysis carried out in the TEM revealed the alumina thin films studied here to be very uniform in composition and that the average composition of the thin films was Al–59.6 ± 2.9 at.% O_2. From these results, it can be concluded that the low temperature reactive evaporation process developed in this study leads to the formation of a continuous nanocrystalline thin film of γ-alumina. Though alumina films have been produced by reactive vapor deposition or by chemical vapor deposition at substrate temperatures above 973 K before,[12,16,17] this is the first report of such a process at low (<700 K) substrate temperatures.

Further evaluation of the nature of the alumina films following annealing was carried out to assess the extent and nature of any interfacial reactions at the alumina/Cr and the Cr/CVDD interfaces. Auger electron spectra were obtained from the alumina film deposited on the {100} crystallite faces of CVD diamond after sputtering off several atomic layers from the surface in order to avoid detection of surface contaminants. Comparison of a typical Auger spectrum from an alumina thin film shown in Fig. 3(a) with the standard spectra of Al_2O_3 [Fig. 3(b), Ref. 31] illustrates clearly that the position and fine structure associated with the Al KLL Auger transition peaks are similar. Characteristic Al peaks appear in the $[dN(E)/(dE)$ vs $N(E)$ plots at 1293, 1331, 1358 (all weak), and 1382 eV (sharp) in the thin film, as compared to those at 1290, 1327, 1355 (all weak), and 1378 eV (sharp) in the Al_2O_3 standard. In contrast, metallic Al is characterized by sharp peaks at 1329, 1345, 1364, 1380, and 1396 eV, as shown in Fig. 3(c).[31] The absence of Auger peaks characteristic of metallic Al confirms that no metallic Al was present in samples prepared by reactive evaporation of Al according to the procedure followed in this study. Auger electron spectra collected from the film after argon-ion sputtering for various periods of time revealed that the spectra collected from various depths within the $\gamma-Al_2O_3$ film were identical to Fig. 3(a), establishing that the thin films were compositionally homogeneous in the thickness direction. A typical Auger depth profile obtained from an alumina thin film deposited on a glass substrate with a Cr interlayer is illustrated in Fig. 3(d). It is observed that the ratio of the peak-to-peak heights of the Al signal to that of the O signal is approximately constant throughout the alumina layer. This clearly demonstrates the chemical homogeneity of the alumina film.

Thus, the electron diffraction and the AES results unambiguously establish that polycrystalline films of $\gamma-Al_2O_3$ can be prepared by vapor deposition of Al at low substrate temperatures (<675 K) in a low oxygen partial pressure environment. This is the first report of such a processing technique that leads to the formation of alumina by a low temperature process in a controlled manner.

D. Structure of the alumina/Cr film deposited on CVD diamond

Figure 4 shows an Auger depth profile through the alumina and Cr films deposited on one of the flat {100}

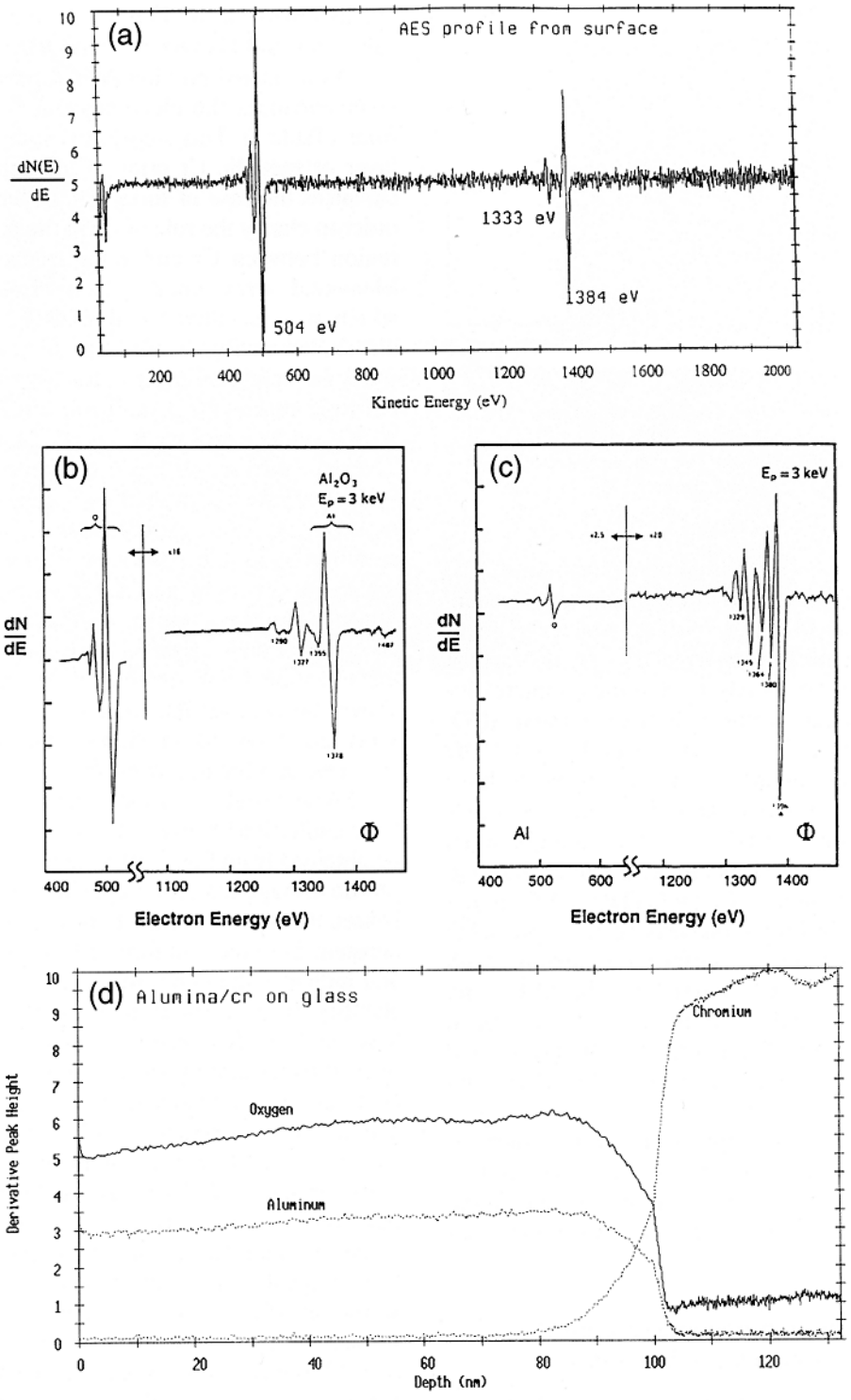

FIG. 3. (a) Auger electron spectrum from the alumina film (after Ar^+ sputtering for 2 min) deposited on CVDD with a Cr interlayer, clearly showing two peaks: one corresponding to oxygen at 504 eV and the other corresponding to aluminum at 1382 eV. The spectrum was obtained from the sample surface after Ar^+ sputtering for a minute and with the primary electron beam energy, E_p, of 5 keV. (b) Oxygen KLL and Al KLL Auger peaks from Al_2O_3[31] and (c) oxygen KLL and Al KLL Auger peaks from pure Al.[31] Notice the similarity in the shape, position, and fine features associated with the peaks in figures (a) and (b). (d) Auger depth profile through an annealed 50 nm Cr/100 nm alumina thin film deposited on glass substrate.

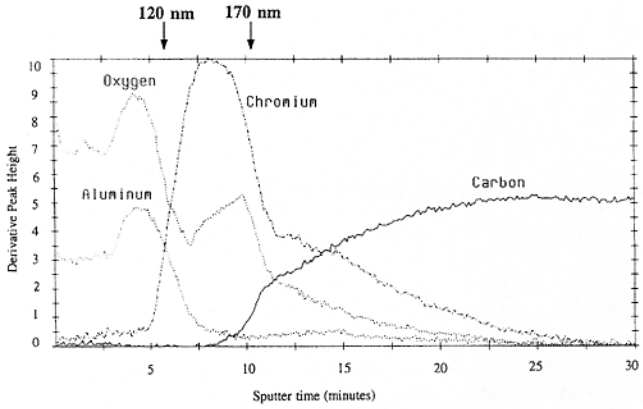

FIG. 4. Auger depth profile through a ~120 nm alumina film deposited on a 50 nm Cr interlayer on a CVDD substrate. The CVDD film was prepared on an AlN substrate. For reference, the thicknesses, where known, are indicated along with the sputter time on the abscissa.

crystallite faces of a CVDD film on polycrystalline AlN. The Al/O ratio is observed to be relatively constant until about 100 nm from the surface (sputter time of ~5 min), in agreement with the TEM results, which showed the layer to be $\gamma-Al_2O_3$. Significant interdiffusion is observed to have occurred between Cr and Al/O. Furthermore, Cr and C from the underlying CVDD are observed to have interdiffused, and appear to have reacted as well. Since two separate interdiffusion zones (one between Cr and CVDD, and the other between Cr and Al-O) are observed in Fig. 4, it can be inferred that following deposition of Cr on CVDD, all Cr is not consumed by carbide formation, leaving an appreciable thickness of free Cr on the surface for bonding with alumina. The interdiffusion zones between Al_2O_3 and Cr and between Cr and C result in strong chemical bonding between Al_2O_3, Cr, and the CVDD layers, and is responsible for the strong adhesion of the Al_2O_3 film to the substrate.

In the following section, the details of the structures of the various interfaces in the multilayered system are explored, and a mechanistic rationalization of the bonding across the Al_2O_3/Cr and Cr/diamond interfaces is sought.

E. Roles of Cr and post-deposition annealing on the formation of alumina thin films

Based on the discussion in Sec. III. D, it is apparent that while part of the Cr deposited on CVDD forms carbide(s) with the underlying diamond, the surface of the as-deposited Cr film consists only of free Cr. It is on this free Cr surface that the alumina film is formed during reactive evaporation of Al and subsequent annealing. Therefore, the microstructure and properties of the alumina film are expected to be independent of the substrate on which Cr is deposited. Hence, the results obtained on alumina/Cr films prepared on glass substrates and CVDD are expected to be equivalent.

As indicated previously, the presence of a Cr interlayer enhances the electrical resistivity of the alumina films (Table I). This suggests that the presence of a thin layer of metallic Cr prior to the deposition of alumina enhances the ease of formation of the alumina phase. In order to clarify the role of Cr in the process, the interface region between Cr and alumina was studied in detail. Elemental x-ray images of a cross-sectional sample, which was metallized with FERRO 3350™ Ag paste, are shown in Fig. 5. For the discussion here, we will focus our attention on the stability of the alumina layer during curing of the metallization at 725 K, and only the Al-K_α, O-K_α, and Cr-K_α x-ray images are presented. The large electron-excited volume in the cross sectional sample masks the true thicknesses of the layers. The most striking result observed here is that separate Cr and alumina layers are observable at the interface between the Ag metallization and diamond, suggesting that the Cr film beneath the alumina is stable despite interdiffusion processes which occurred during the annealing and the metallization firing treatments. However, as mentioned above, because of the limited spatial resolution of the x-ray maps, no information on the extent of interdiffusion can be obtained from these results.

Some insight into the extent of interdiffusion (and hence adhesion) between the Cr and alumina layers can be obtained from Fig. 3(d), which shows the Auger depth profile through the films deposited on a glass substrate. It is seen that the aluminum to oxygen ratio remains nearly constant from the thin film surface to a depth of ~87 nm and indicates the compositional uniformity and also the stability of the microstructure at temperatures below at least <675 K. Between ~87 nm and 100 nm, substantial interdiffusion among Al, Cr, and O is observed to have occurred. A careful examination of the Auger line shapes and positions associated with the Cr LMM, O KLL, and the Al KLL transitions in the overlying Al_2O_3, in the interfacial layer between Al_2O_3 and Cr, and in the underlying Cr layer [Figs. 6(a) and 6(b)] showed that while the main Cr LMM peak remained at 529 eV, the O-KLL peak shifted from 504 in alumina to 506 eV at the interface while the main Al peak at 1382 eV shifted by 1 eV. The absence of a sharp Auger peak at ~1396 eV clearly indicates that metallic Al is not present in these samples. This is in contrast to the observations of Lu *et al.*[21] on Cr deposited on sapphire (or 99.6% alumina) annealed at 973 K under ultrahigh vacuum conditions. As discussed in Sec. I, based on the observation of Auger peaks ~1395 eV, Lu *et al.*[21] propose that the alumina is reduced by Cr to metallic Al at the interface during the production of Cr_2O_3. However, this suggested reduction reaction is thermodynamically improbable since the free energy of formation

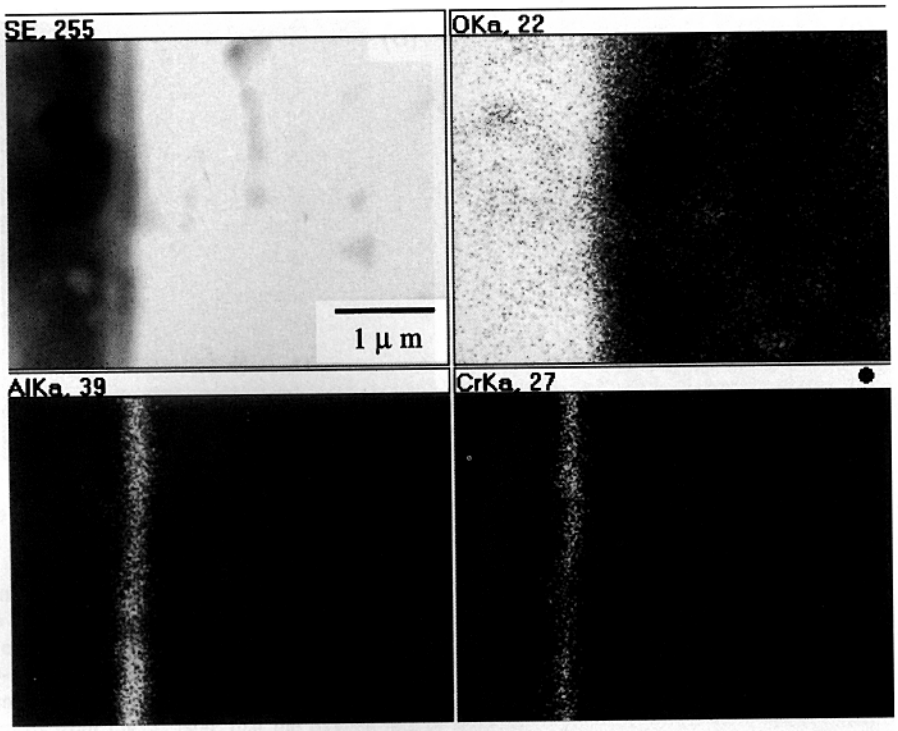

FIG. 5. Cross section of a 125 nm alumina film on glass substrate with 75 nm Cr intermediate layer after metallization with FERRO 3350™ Ag paste. Secondary electron image (top left) and O-K_α, Al-K_α, and Cr-K_α x-ray images as indicated. The glass substrate is on the left and the Ag metallization is to the right of the alumina layer.

of Al_2O_3 is less than that of Cr_2O_3 (i.e., $\Delta G_{Al_2O_3} < \Delta G_{Cr_2O_3}$) at all temperatures below 9262 K.[32] It appears more plausible that the interface region between the Cr and the alumina layer is comprised of either a solid solution or a two phase mixture of chromium oxide and aluminum oxide. This possibility is strongly supported by the phase diagram of Al_2O_3–Cr_2O_3,[33] which exhibits unlimited solid solubility between Al_2O_3 and Cr_2O_3 at temperatures above 1070 K, and the existence of a miscibility gap below this temperature.

In order to determine the structure of the Cr/Al_2O_3 interfacial region, a 25 nm Cr/75 nm alumina film deposited on {100} NaCl and annealed at 675 K for 24 h, was separated from the substrate and examined in the TEM. The contrast variations seen in the bright-field micrograph shown in Fig. 7(a) shows that the microstructure is clearly two-phase and is similar to that of a spinodally evolved microstructure in a near-zero elastic misfit system. Al, O, and Cr electron energy loss (EEL) images obtained from an area such as Fig. 6(a) would show random distribution of all the elements if they existed as a single solid solution, whereas Al and Cr will appear segregated (with O distributed randomly) if the two oxide phases co-existed. On the other hand, O would be absent from any region where pure Al or Cr may be present. Figures 7(b) and 7(c) show Al-L and O-K elemental EEL maps, respectively. The bright areas in Fig. 6(b) indicate the areas that are Al-rich

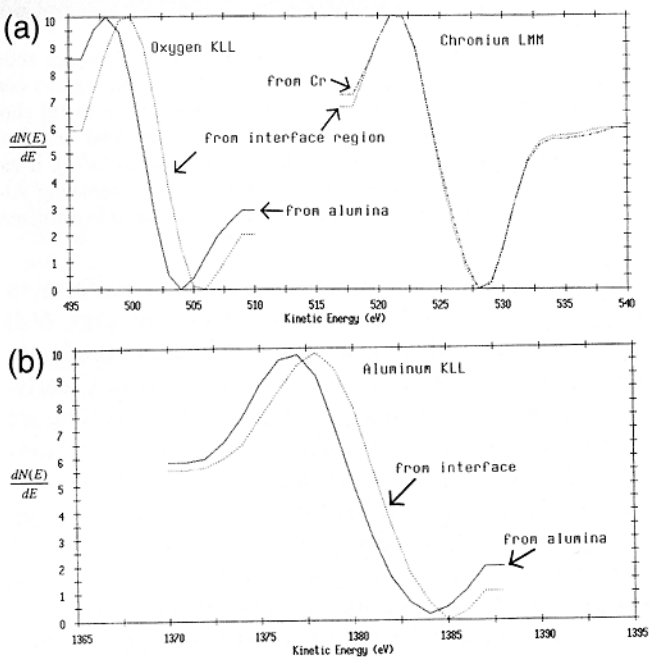

FIG. 6. Comparison of the Auger line profiles from the Cr/alumina interface with those from alumina or Cr. Same sample as in Fig. 3(d). (a) O KLL and Cr LMM and (b) Al KLL. The spectra from the interface regions are plotted in dotted lines. The spectra from pure alumina, interface, and pure Cr shown here were obtained by Ar^+ sputtering for 9, 23, and 40 min, respectively.

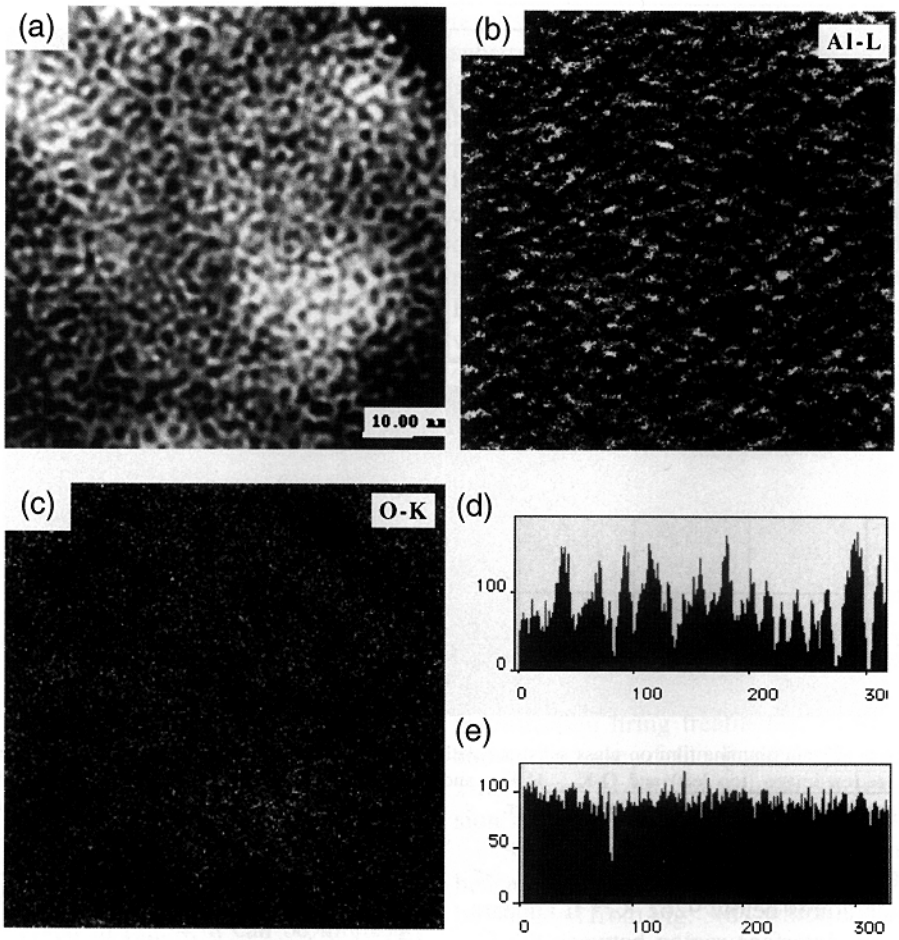

FIG. 7. (a) Zero loss energy filtered (slit width of 5 eV) image showing the typical appearance of the annealed alumina film deposited on a 25 nm Cr interlayer. The dark and bright interconnected regions correspond to alumina-rich and alumina-poor (hence chromia-rich) regions, respectively. (b) Al-L elemental map from region shown in (a) showing that the microstructure comprises of regions alternately rich in Al and poor in Al (and hence rich in Cr). (c) O-K elemental map from region shown in (a) showing that oxygen is uniformly distributed in the microstructure. Combining the information from (a) to (c), it can be deduced that the bright regions in (a) are rich in chromium oxide. (d) Line profile obtained from (b) aids in seeing the alternating Al-rich and Al-poor regions in (b). (e) Line profile obtained from (c) aids in seeing that oxygen is uniformly distributed in the microstructure shown in (a).

while the distribution of O appears quite uniform in Fig. 6(c). This point is again illustrated in Figs. 6(d) and 6(e), where plots of the intensities along randomly drawn lines in Figs. 6(b) and 6(c) are shown. Clearly, the microstructure contains alternating regions that are Al-rich and Al-poor. Undoubtedly, the Al-poor regions are richer in Cr than the Al-rich regions. Since the pre-edge images used to calculate the Cr-L elemental map (the onset of the L_3 edge of Cr is at 575 eV) overlaps with the K edge of O (onset at 532 eV), it was not possible to obtain good quality Cr elemental images.

Further insight into the microstructures of the film prior to, and following annealing can be obtained from the EELS results. EEL spectra were obtained from various alumina thin films, prepared with or without a Cr interlayer in the as-deposited condition (i.e., without post-deposition annealing), or after annealing. Typical electron energy loss spectra near the O-K edge from samples under three different conditions are presented in Fig. 8. The spectrum from the pure alumina sample (top-most curve) shows O-K edge characteristic of alumina in agreement with previous work.[34] The spectrum from Cr regions shown in the bottom curve exhibits the $L_{2,3}$ edges characteristic of Cr metal at ~575 and ~584 eV apart from a very weak oxygen edge. The spectrum from annealed Cr/alumina sample shown by the middle curve shows the Cr $L_{2,3}$ edges again at ~575 and ~584 eV as well as two oxygen K edges at ~529 and ~532 eV. A careful comparison of the Cr $L_{2,3}$ edges from the as-deposited and annealed samples reveals two noticeable features: (a) the threshold for edge onset is shifted to slightly higher energies in the annealed sample and (b) the shape of the white lines appear more symmetric in the annealed sample. Both these observations are in agreement with that reported by Leapman *et al.*[35] for the case of metallic Cr and Cr_2O_3, with the L_3 and the L_2

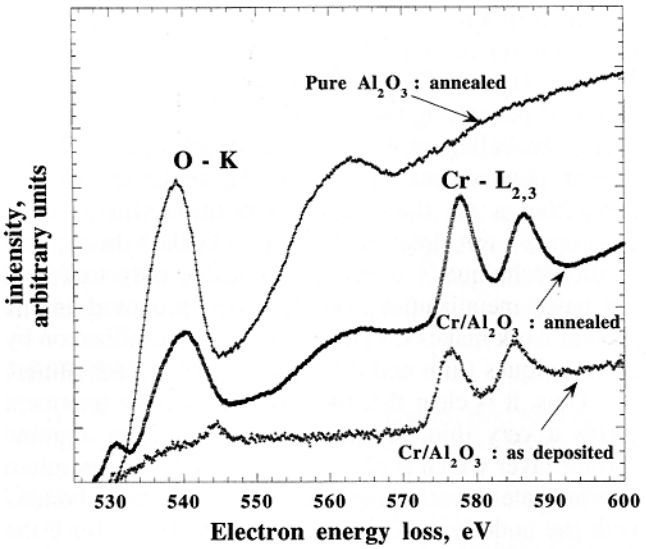

FIG. 8. Typical electron energy loss spectra from three different thin films as described in the legend. The topmost curve shows a strong O-K edge at ~533 eV characteristic of pure alumina. The middle curve shows two O-K edges in the annealed Cr/alumina sample, confirming the presence of two oxides present in the microstructure supporting the inferences from Fig. 7. Note that the oxygen pickup during the deposition of Cr is very small (presumably O is in solid solution or as an interstitial impurity) as indicated by a weak O-K edge in the bottom-most curve. Notice also that the K edge associated with the dissolved oxygen appears at a higher energy than that associated with the oxide in Cr.

edges in Cr being asymmetrical, rising more abruptly on the low energy side and L_3 appearing at 575 eV. The L_3 edge in Cr_2O_3 appears at 576 eV and both the edges are nearly symmetrical. Thus, fine structure information from the samples studied here indicate that whereas metallic Cr is present in the as-deposited sample, it reacts with the oxygen during the annealing process to produce Cr_2O_3, resulting in the interpenetrating two-phase mixture of alumina and chromia in the region near the Cr-alumina interface.

It is important to note that even after this interdiffusion, there remains a pure Cr layer underneath the alumina as demonstrated earlier from EDS (Fig. 5) and Auger microprobe experiments [Fig. 4(d)]. This suggests that when a similar multilayered thin film is prepared on a CVDD surface, the transition metal buffer layer should be present between the CVDD and the alumina layers. This is important since the incorporation of the Cr layer below the alumina layer, which increased the stability of the alumina, may also act as the carbide-forming element that provides good chemical bonding with the diamond surface.

In order to confirm the formation of the chromium carbide at the CVDD/Cr interface, thin films of pure Cr deposited on CVDD substrates, subjected to a 24 h annealing treatment at 673 K at a chamber pressure of less than 10^{-7} Torr, were examined by AES. Figure 9(a)

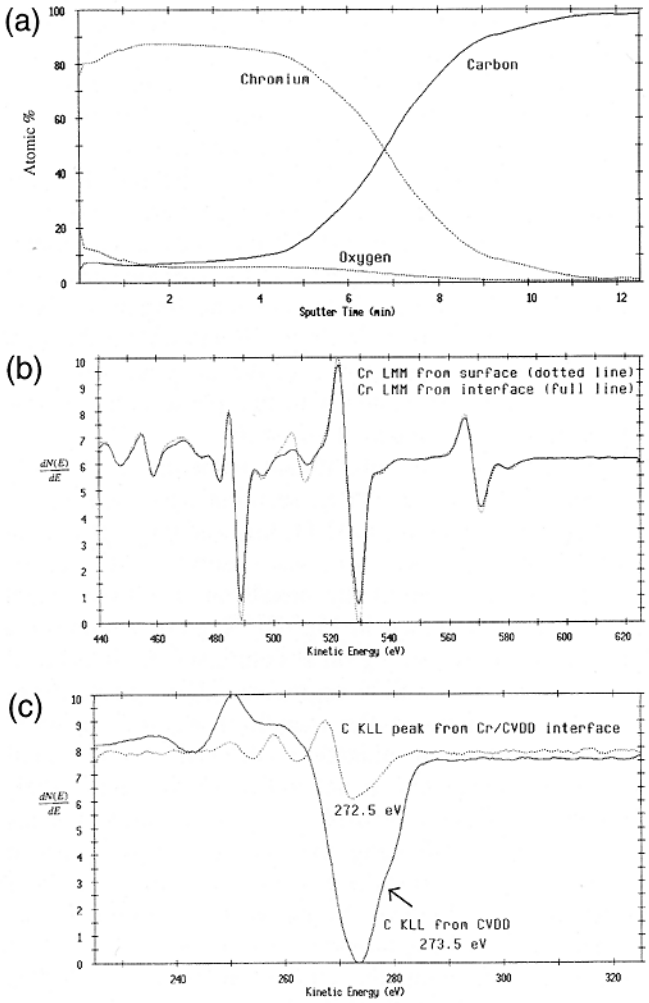

FIG. 9. Auger spectroscopy results on a sample containing 125 nm Cr deposited on CVDD and subsequently annealed at 645 K for 24 h. (a) Typical Auger depth profile showing Cr and C interdiffusion. Auger profiles of (b) Cr LMM and (c) C KLL from the interface (dotted lines) and bulk Cr or diamond. The bulk Cr, interface, and bulk diamond profiles were obtained after Ar^+ sputtering for 1.5, 5.3, and 10 min, respectively.

illustrates a typical depth profile obtained from the annealed CVDD/Cr couple indicating a distinct diffusion zone at the interface. As clear from Fig. 9(a), little oxygen is incorporated in the Cr film from the chamber atmosphere. Comparison of Cr LMM and C KLL Auger spectra from the interface region and those from the metallic Cr film and from CVDD [presented in Figs. 9(b) and 9(c), respectively] clearly suggest a chemical reaction between Cr and C in the interface region. The Auger peaks associated with Cr in the metallic state and those from the interface region appear identical [Fig. 9(b)], but it is difficult to draw any conclusion from this about the chemical changes associated with Cr at the interface. However, examination of the features corresponding to the KLL transition associated with carbon [Fig. 9(c)] provides significant information.

The Auger spectrum from CVDD is characterized by a peak at 273.5 eV [Fig. 9(c), and Ref. 36], while that from the Cr/CVDD interface exhibits three peaks at 252 eV, 262 eV, and 272.5 eV. According to the Cr-C phase diagram, Cr forms three different carbides: $Cr_{23}C_6$, Cr_7C_3, and Cr_3C_2. A comparison of the fine features associated with the spectra presented here [Figs. 9(b) and 9(c)] with those reported from various chromium carbides[37,38] strongly suggest that the carbide formed at the CVDD/Cr interface following annealing at 675 K is $Cr_{23}C_6$. The formation of $Cr_{23}C_6$ is in conformity with the thermodynamic properties of the Cr–C system since the free energy associated with this phase is the lowest of the three Cr-carbides at 675 K.[39]

In order to further investigate the nature of the CVD diamond-Cr interface, a cross-sectional specimen of diamond coated with the Cr/Al_2O_3 film and metallized with DuPont DC101™ Au paste was observed in the TEM. A bright-field image of the metallization CVDD interfacial region is shown in Fig. 10. Region A represents the CVDD substrate, region B comprises the interfacial Al_2O_3/Cr layer as well as segregated glassy phases from the frits contained in the metallization, and region C represents the Au metallization. Although the individual Cr and alumina layers are not apparent in the figure, their existence has been verified by detailed microanalysis of region B,[40] indicating the stability of the surface treatment. Thus, the surface modification proposed here is chemically stable even in the presence of molten frits at metallization firing temperatures as high as 1075 K. It is clear from the figure that chromium carbide crystallites are present at the CVDD/Cr interface, represented by the boundary between regions B and A. Transition metal carbide formation at transition metal/diamond interfaces has been reported previously for various metals like V, Mo, Ti, Hf, Ta, Nb, and W, either during CVD diamond processing on refractory metal substrates,[41] or during annealing of CVDD/Mo samples at 1223 K.[29] It was pointed out by one of the reviewers of this paper that a Au thick film composition was recently developed[42] for direct application to CVDD. In contrast to this technique,[42] which is applicable only to fritted Au paste metallization, the approach proposed in the present work makes CVDD amenable to metallization by all techniques (thin and thick film) suitable for alumina.

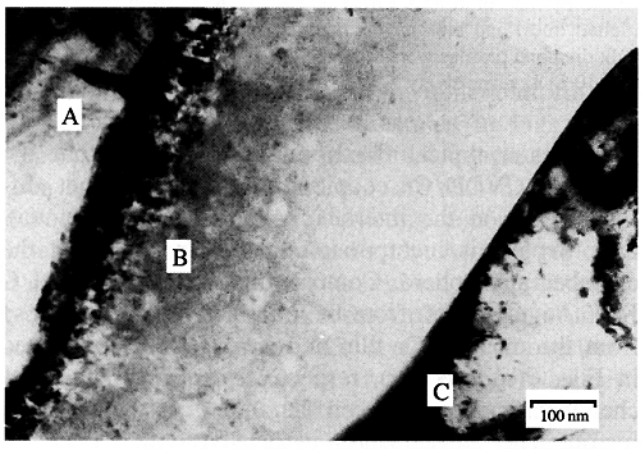

FIG. 10. Bright-field micrograph illustrating the typical appearance of the cross section of an Au-metallized alumina/Cr/CVDD/AlN sample. Regions marked A and C correspond to the CVDD and the Au layers, respectively. Region B comprises the alumina/Cr layer as well as the glassy layer originating from the metallization heat treatment. Notice the thin layer containing crystals of chromium carbide between layers A and B.

Thus, it is clear that the proposed surface treatment yields a very thin, ultrafine-grained, adherent alumina surface layer which is chemically bonded to a chromium intermediate layer, which in turn chemically bonded with the underlying CVD diamond substrate. Since the surface layer is alumina, which is widely used as a substrate material for electronic packaging, the CVD diamond substrate, treated as above, is expected to be easily metallizable by a number of thin and thick film techniques, using existing materials and procedures developed for alumina.

IV. CONCLUSIONS

(1) A simple procedure for the deposition of nanocrystalline alumina thin films on synthetic diamond at low temperatures has been described. The procedure consists of evaporative deposition of a thin (~50 nm) layer of Cr in vacuum followed by reactive evaporation of Al in $\sim 10^{-4}$ Torr oxygen on a substrate heated to <675 K and a post-deposition annealing in ~500 Torr oxygen at ~675 K for ~24 h.

(2) The alumina film produced is nanocrystalline with a grain size of 3–25 nm and has the crystal structure of γ–Al_2O_3 and has a uniform composition throughout the thickness of the thin film.

(3) The presence of Cr substantially increases the ease of formation of alumina. TEM studies have shown that a fine two-phase microstructure comprising of an intimate mixture of Al_2O_3 and Cr_2O_3 forms at the Cr/Al_2O_3 interface, resulting in strong adhesion across the interface.

(4) The synthetic diamond reacts with the metallic Cr during the processing stage to produce $Cr_{23}C_6$ at CVDD/Cr interface, yielding a strong bond between Cr with diamond.

(5) Finally, since the surface treatment detailed here produces a continuous polycrystalline alumina layer, it is expected to render CVD diamond metallizable by various conventionally utilized thin and thick film approaches developed for alumina packaging, and obviate the need to pattern any adhesion-enhancing interlayer identically to the interconnection material, while result-

ing in negligible deterioration of the through-thickness thermal conductivity of the substrate.

ACKNOWLEDGMENTS

This work was supported by a grant from the Naval Surface Warfare Center, Crane Division, Indiana, with K. G. Beasley and C. W. Sims as contract monitors. The authors wish to express their gratitude to Dr. J. Sosniak of Naval Air Warfare Center, Aircraft Division, Indianapolis, for supplying the CVDD substrates.

REFERENCES

1. D. J. Pickrell, P. J. Santini, and F. M. Kimock, Proc. Int. Symp. on Microelectronics, Vol. 2105 (The Microelectronic Society, 1993), p. 405.
2. C. D. Iacovangelo and E. C. Jerabek, in Proc. Int. Symp. Microelectronics, Dallas, TX (1993), pp. 132–137.
3. C. D. Iacovangelo, P. J. DiConza, E. C. Jerabek, and K. P. Zarnoch, in *Advanced Metallization for Devices and Circuits–Science, Technology, and Manufacturability,* edited by S. P. Murarka, A. Katz, K. N. Tu, and K. Maex (Mater. Res. Soc. Symp. Proc. **337**, Pittsburgh, PA, 1994), pp. 401–412.
4. C. D. Iacovangelo, E. C. Jerabek, R. H. Wilson, and P. C. Schaefer, U.S. Patent No. 5,328,715 (1994).
5. W. C. Dautremont-Smith, L. C. Feldman, R. Kalish, A. Katz, B. Miller, and N. Moriya, U.S. Patent No. 5,334,306 (1994).
6. K. P. Zarnoch and C. D. Iacovangelo, U.S. Patent No. 5,346,719 (1994).
7. C. D. Iacovangelo, E. C. Jerabek, R. H. Wilson, and P. C. Schaefer, U.S. Patent No. 5,382,758.
8. E. S. K. Menon and I. Dutta, Appl. Phys. Lett. **68**, 2951 (1996).
9. I. Dutta and E. S. K. Menon, U.S. Patent Application No. NC 77524 (1997).
10. E. Ritter, L. R. Kaminski, and K. Hohenegger, U.S. Patent No. 4,172,156 (1979).
11. R. S. Nowicki, J. Vac. Sci. Technol. **14**, 127 (1977).
12. R. F. Bunshah and R. J. Schramm, Thin Solid Films **40**, 211 (1977).
13. C. A. T. Salama, J. Electrochem. Soc. **117**, 913 (1970).
14. R. F. Bunshah and A. C. Raghuram, J. Vac. Sci. Technol. **9**, 1385 (1972).
15. D. Hoffman and D. Leibowitz, J. Vac. Sci. Technol. **8**, 107 (1971).
16. E. M. DaSilva and P. White, J. Electrochem. Soc. **109**, 12 (1962).
17. E. Ferrieux and B. Pruneaux, J. Electrochem. Soc. **116**, 1008 (1969).
18. E. Kay, in *Techniques of Metals Research,* edited by R. F. Nunshah (Wiley, New York, 1968), Vol. 1.
19. L. Holland, *Vacuum Deposition of Thin Films* (Chapman and Hall, London, 1966).
20. D. S. Campbell, *Handbook of Thin Film Technology* (McGraw Hill, New York, 1970).
21. H. Lu, Y. D. Cui, J. Qin, C. L. Bao, and D. H. Shen, Appl. Surface Sci. **103**, 113 (1996).
22. S. S. Perry, J. W. Ager, G. A. Somorjai, R. J. McClelland, and M. D. Drory, J. Appl. Phys. **74**, 7542 (1993).
23. X. L. Peng and T. W. Clyne, Thin Solid Films **312** (1–2), 213 (1998).
24. W. Zhu, P. C. Yang, and J. T. Glass, Appl. Phys. Lett. **63**, 1640 (1993).
25. Y. Tzou, J. Bruley, F. Ernst, and M. Rühle, J. Mater. Res. **9**, 1566 (1994).
26. T. Tachibana and J. T. Glass, Diamond Relat. Mater. **2**, 963 (1993).
27. C. D. Iacovangelo, Thin Solid Films **286**, 264 (1996).
28. W. D. Brown, H. A. Naseem, A. P. Malshe, J. H. Glezen, and W. D. Hinshaw, in *Materials Reliability in Microelectronics V,* edited by A. S. Oates, K. Gadepally, R. Rosenberg, W. F. Filter, and A. L. Gries (Mater. Res. Soc. Symp. Proc. **391**, Pittsburgh, PA, 1995), p. 59.
29. K. L. Moazed, J. R. Ziedler, and M. J. Taylor, J. Appl. Phys. **68**, 2246 (1990).
30. I. Meyyappan, A. P. Malshe, H. A. Naseem, and W. D. Brown, Thin Solid Films **253**, 407 (1994).
31. L. E. Davis, N. C. McDonald, P. W. Palmberg, G. E. Riach, and R. E. Weber, *Handbook of Auger Electron Spectroscopy* (Physical Electronics, 1976).
32. D. R. Gaskell, *Introduction to Metallurgical Thermodynamics,* 2nd ed. (McGraw Hill, New York, 1981).
33. E. M. Levin, C. R. Robbins, and H. F. McMurdie, *Phase Diagrams for Ceramists,* edited by M. K. Reser (American Ceramics Society, Westerville, OH, 1964), Fig. 309; R. Roth, T. Negas, and L. P. Cook, *Phase Diagrams for Ceramists,* Vol. IV, edited by G. Smith (American Ceramics Society, Westerville, OH), Fig. 5189.
34. C. C. Ahn and O. L. Krivanek, *EELS Atlas: A reference guide of electron energy loss spectra covering all stable elements,* Arizona State University HREM facility/GATAN Inc., 1993.
35. R. D. Leapman, L. A. Grunes, and P. L. Fejes, Phys. Rev. B **26**, 614 (1982).
36. M. L. Terranova, V. Sessa, R. Bernardini, I. Davoli, and M. De Crescenzi, Surf. Sci. **331–333**, 1050 (1995).
37. *Practical Surface Analysis,* edited by D. Briggs and M. P. Seah, 2nd ed. (John Wiley & Sons, New York, 1990), Vol. 1, p. 102.
38. S. Danyluk, J. Y. Park, and D. E. Busch, Scripta Metall. **13**, 857 (1979).
39. E. T. Turkdogan, *Physical Chemistry of High Temperature Technology* (Academic Press, New York, 1980), p. 10.
40. E. S. K. Menon and I. Dutta, unpublished research.
41. S. D. Wolter and J. T. Glass, J. Appl. Phys. **77**, 5119 (1995).
42. J. Crumpton, R. Koba, K. Valenta, B. Speck, C. Roach, D. Kuty, and R. Keusseyan, MCM Conference 1997.